An Assessment of the Impact of Uncertainty on Automatic Generation Control Systems

Dimitra Apostolopoulou, *Member*, *IEEE*, Alejandro D. Domínguez-García, *Member*, *IEEE*, and Peter W. Sauer, *Fellow Member*, *IEEE*

***Abstract*—This paper proposes a framework to quantify the impact of uncertainty that arises from load variations, renewable-based generation, and noise in communication channels on the automatic generation control (AGC) system. To this end, we rely on a model of the power system that includes the synchronous generator dynamics, the network, and the AGC system dynamics, as well as the effect of various sources of uncertainty. Then, we develop a method to analytically propagate the uncertainty from the aforementioned sources to the system frequency and area control error (ACE), and obtain expressions that approximate their probability distribution functions. We make use of this framework to obtain probabilistic expressions for the frequency performance criteria developed by the North American Electric Reliability Corporation (NERC); such expressions may be used to determine the limiting values of uncertainty that the system may withstand. The proposed ideas are illustrated through the Western Electricity Coordination Council (WECC) 9-bus 3-machine system and a 140-bus 48-machine system.**

***Index Terms*—Automatic Generation Control, Renewable-based Generation, Noise in Communication Channels, Stochastic Differential Equation Model, Frequency Performance Criteria**

I. Introduction

To ensure the reliable operation of a power system, generation needs to meet demand and the system frequency needs to be kept as close as possible to the nominal value at all times. These tasks are met via load frequency control (LFC), which includes several control systems that are implemented across different time scales. One such system is the automatic generation control (AGC), the role of which is to maintain system frequency and the real power interchange between balancing authority (BA) areas to desired values. Most BA areas implement tie-line bias control, and the AGC command is driven by the value of the area control error (ACE), which includes the deviation of the sum of the tie line flows between BA areas, and their obligation to support frequency.

At the same time, power systems are undergoing radical transformations, which are enabled by the integration of new technologies, such as advanced communication, and renewable-based generation. However, it is not clear if current AGC system implementations are suitable for handling the challenges that may arise due to these transformations [1]. For example, it is not obvious whether or not current AGC systems will be able to deal with increased uncertainty arising from sources other than just load variations, e.g., renewable-based generation mandated by several policies (see, e.g., [2]). Furthermore, the AGC system accepts measurements of the real power interchange between BA areas, the area frequency, and generator output as inputs from field devices and processes them to obtain the generator control commands. In this regard, increased noise in the communication channels that the AGC system relies on might affect its performance [3].

In North America, the performance of the AGC system is evaluated by three performance criteria, CPS1, CPS2, and BAAL, defined by the North American Electric Reliability Corporation (NERC). More specifically, CPS1 and CPS2, respectively, are statistical measures of the ACE variability and magnitude [4]. The BAAL criterion is designed to replace CPS2 since the latter often gives the BA area the indication to move its ACE opposite to what helps keeping frequency at its nominal value. This problem is overcome in the BAAL criterion by establishing frequency-dependent ACE limits [5].

Given these additional sources of uncertainty from load variations, renewable-based generation, and noise in communication channels, there is a need to investigate if present AGC system implementations are sufficient for meeting NERC performance standards, and to determine their limitations. To this end, this paper proposes a framework to evaluate the effects of the aforementioned sources of uncertainty, and to assess the AGC system behavior. The adopted modeling framework includes synchronous generator dynamics, the AGC system dynamic behavior, and the effect of the aforementioned uncertainty sources. We use the framework to approximate the probability distribution functions (pdfs) of system variables of interest, which in turn will be used to obtain probabilistic expressions of the three aforementioned performance criteria. In this context, we may explore if reliability criteria are met under different scenarios for each of the uncertainty sources. For example, we may investigate whether or not the functionality provided by current AGC systems is appropriate for dealing with high levels of renewable-based generation combined with noise in communication channels. In this paper, we numerically verified that the solutions provided by the proposed framework, as well as, the probabilistic expressions for frequency performance criteria, are sufficiently accurate.

Next, we discuss some relevant works in the literature which

The authors are with the Department of Electrical and Computer Engineering of the University of Illinois at Urbana-Champaign, Urbana, IL 61801, USA. E-mail: {apostol2, aledan, psauer}@illinois.edu.

The work of Apostolopoulou and Sauer was supported in part the US Departments of Energy and Homeland Security through the Trustworthy Cyber Infrastructure for the Power Grid, the US Department of Energy GEARED Initiative, the Power Systems Engineering Research Center (PSERC), and the Grainger Foundation Endowments to the University of Illinois. The work of Domínguez-García was supported in part by the National Science Foundation (NSF) under CAREER Award ECCS-CAR-0954420 and NSF award ECCS-CPS-1135598.

have also looked at the effects that new technologies being introduced in the grid may have on frequency regulation. The analysis of the impact that small wind turbines might have on load frequency control, and in particular AGC systems, is studied in [6]. A robust controller that copes with communication delays and other problems in the communication network and ensures good performance of load frequency control is given in [7]. The analysis of the system behavior in the case an attacker gains access to the AGC signal and injects undesirable inputs to the system is studied in [8]; in this work the authors propose the design of an optimal control strategy to destabilize a two-area power system in the case such a cyber attack occurs. In [9], the authors propose a stochastic optimal relaxed AGC system, which takes into account NERC's frequency performance standards, and reduces control cost by tuning the relaxation factors online. In [10], the authors formulate the frequency regulation problem by viewing future electric power networks as a general dynamical system driven by disturbances, and propose a modified AGC system that better responds to fast disturbances. A method to determine the impact of random load perturbations on system stability by calculating the evolution of the probability density function of system states with the Fokker-Planck equation is presented in [11]. In [12], the authors motivate the need for stochastic models in power system analysis and propose a systematic approach that describes power system behavior as continuous stochastic differential-algebraic equations. In [13], the authors propose a framework to study the impact of stochastic power injections (e.g., arising from renewable-based generation) on power system dynamics. In [14], a study that investigates how individual wind turbines affect the wind farm performance under the AGC set-point operation is presented.

The remainder of the paper is organized as follows. In Section II, we describe the power system model that we adopt to develop our analysis framework. In Section III, we demonstrate how uncertainty arising from load variations, renewable-based generation, and noise in communication channels can be handled, and derive the proposed framework. In Section IV, we make use of the framework to obtain probabilistic expressions of the frequency performance criteria. In Section V, we illustrate the methodology through the Western Electricity Coordination Council (WECC) 9-bus 3-machine system and a 140-bus 48-machine system. In Section VI, we summarize the results and make some concluding remarks.

II. Power System Model

In this section, we introduce the non-linear and linearized power system dynamic models that we utilize to develop our framework. More specifically, we introduce dynamic models for synchronous generators, wind-based generators, and the AGC system; and the network model.

A. Non-Linear Model

1) Synchronous generators: For the timescales of interest in this paper, we choose a 9-state model (see, e.g., [15]). The state vector for generator i is denoted by x_i, whereas P_{C_i} denotes the AGC command signal this generator receives from the system operator when participating in frequency regulation. We also denote by I_{d_i} (I_{q_i}) the d-axis (q-axis) component of the stator current, θ_i the voltage angle, and V_i the voltage magnitude at bus i. Consider a network with n buses and I generators, and define $x = [x_1^T, \ldots, x_I^T]^T$ and $u = [P_{C_1}, \ldots, P_{C_I}]^T$. In addition, we define the vector of machine algebraic variables as $\tilde{y} = [\tilde{y}_1^T, \ldots, \tilde{y}_I^T]^T$, where $\tilde{y}_i = [I_{d_i}, I_{q_i}]^T$; and we define the vector of network variables $y = [y_1^T, \ldots, y_n^T]^T$, where $y_i = [\theta_i, V_i]^T$. Then, the dynamic behavior of the synchronous generators can be described by

$$\dot{x} = f(x, y, \tilde{y}, u), \tag{1}$$

$$0 = g_1(x, y, \tilde{y}); \tag{2}$$

a detailed description of this model and the precise form that f and g_1 take may be found in [15, p. 140].

2) Wind-based generation: We assume a first order dynamical model, which has been shown to provide an accurate relationship between the wind speed and the real power generated by a collection of wind turbines (see, e.g., [16]). Such a model is derived from a 7-state two-axis model of a WECC of type III, i.e., a doubly-fed induction generator. The derivation is accomplished via selective modal analysis, and the resulting model only maintains one mode, which is sufficient for studying the phenomena of interest in the paper. We denote by P_{W_i} (Q_{W_i}) the wind-based active (reactive) generation at bus i. We assume that $Q_{W_i} = 0$ for all wind-based generation. Then, the dynamic behavior of the wind-based generation at bus i is given by

$$\dot{P}_{W_i} = \varrho_{1_i} P_{W_i} + \varrho_{2_i} v_i + \varrho_{3_i}, \tag{3}$$

where v_i is some average wind speed at bus i, and ϱ_{1_i}, ϱ_{2_i} and ϱ_{3_i} are parameters that depend on characteristics of the wind-based generators. We denote the vector of wind-based generation by $P_W = [P_{W_1}, \ldots, P_{W_n}]^T$ and the vector of wind speeds by $v = [v_1, \ldots, v_n]^T$. Then, we have

$$\dot{P}_W = q(P_W, v). \tag{4}$$

3) AGC system: We assume that there are $m = 1, 2, \ldots, M$ BA areas within an interconnected system, and denote by $\mathscr{G}_m$ the set that indexes the generators in BA area m. Then, we take the frequency of BA area m to be

$$f_m = \frac{1}{2\pi} \sum_{i \in \mathscr{G}_m} \gamma_i \omega_i = \frac{1}{2\pi} \frac{\sum_{i \in \mathscr{G}_m} H_i \omega_i}{\sum_{i \in \mathscr{G}_m} H_i}, \tag{5}$$

where H_i is the inertia constant for generator i. We denote by $\mathscr{A}_m$ the set of BA areas that have transmission lines connected to BA area m. Then, the ACE for BA area m is given by

$$ACE_m = \sum_{m' \in \mathscr{A}_m} (P_{mm'} - P_{mm'_{sch}}) - b_m(f_m - f_{\text{nom}}), \tag{6}$$

where $b_m < 0$ is the frequency bias factor for BA area m, f_{nom} is the nominal frequency, $P_{mm'}$ is the power transfer from BA area m to BA area m', which is positive for exporting, and $P_{mm'_{sch}}$ is the scheduled power transfer from BA area m to BA area m'.

Let z_m denote the sum of the AGC commands sent to generators in BA area m, i.e., $\sum_{i\in\mathscr{G}_m} P_{C_i}$; then, following [17, p. 352-355], we have that

$$\dot{z}_m = -z_m - ACE_m + \sum_{i\in\mathscr{G}_m} P_{G_i}, \tag{7}$$

where P_{G_i} is the real power generated by the synchronous generator connected to bus i. Each generator $i \in \mathscr{G}_m$ participates in AGC with $P_{C_i} = \kappa_{m_i} z_m$, where the κ_{m_i}'s are the so-called participation factors, and satisfy the relation $\sum_{i\in\mathscr{G}_m} \kappa_{m_i} = 1$ [18], [19]. We denote the vector of AGC states by $z = [z_1, \ldots, z_M]$. Thus, the dynamic behavior of the AGC system is given by

$$\dot{z} = h(x, y, \tilde{y}, z), \tag{8}$$

$$u = k(z). \tag{9}$$

4) Network: Unlike traditional AGC models (see, e.g., [17]), in this work, we explicitly consider the network model; this way, we are capturing the effect that the network has on the overall closed-loop system dynamic behavior. Let P_{L_i} (Q_{L_i}) represent the active (reactive) power load at bus i and the vector of loads is denoted by $P_L = [P_{L_1}, \ldots, P_{L_n}]^T$ and $Q_L = [Q_{L_1}, \ldots, Q_{L_n}]^T$; then we have that

$$0 = g_2(x, y, \tilde{y}, P_L, Q_L, P_W). \tag{10}$$

The overall system dynamic behavior, including the AGC system, is described by the differential algebraic equation (DAE) system given by (1)-(2), (4), and (8)-(10). The functions f, h, q, k, g_1, and g_2 are assumed to be continuously differentiable with respect to their arguments.

B. Linearized Model

For the timescales of interest, we assume that disturbances introduce a small error to the nominal system trajectory $(x^\star, y^\star, \tilde{y}^\star, u^\star, z^\star, P_W^\star, v^\star, P_L^\star, Q_L^\star)$. Thus, the actual system dynamic behavior can be approximated by linearizing the DAE model in (1)-(2), (4), and (8)-(10) along $(x^\star, y^\star, \tilde{y}^\star, u^\star, z^\star, P_W^\star, v^\star, P_L^\star, Q_L^\star)$. Then, sufficiently small deviations around the system nominal trajectory may be approximated by

$$\Delta\dot{x} = A_1(t)\Delta x + A_2(t)\Delta y + A_3(t)\Delta\tilde{y} + B_1(t)\Delta u, \tag{11}$$

$$\Delta\dot{P}_W = \varrho_1(t)\Delta P_W + \varrho_2(t)\Delta v, \tag{12}$$

$$\Delta\dot{z} = A_4(t)\Delta x + A_5(t)\Delta y + A_6(t)\Delta\tilde{y} + A_7(t)\Delta z, \tag{13}$$

$$\Delta u = B_2(t)\Delta z, \tag{14}$$

$$0 = C_1(t)\Delta x + C_2(t)\Delta y + C_3(t)\Delta\tilde{y}, \tag{15}$$

$$0 = C_4(t)\Delta x + C_5(t)\Delta y + C_6(t)\Delta\tilde{y} + D_1(t)\Delta P_L + D_2(t)\Delta Q_L + D_3(t)\Delta P_W, \tag{16}$$

where the matrices $A_1(t)$, $A_2(t)$, $A_3(t)$, $A_4(t)$, $A_5(t)$, $A_6(t)$, $A_7(t)$, $B_1(t)$, $B_2(t)$, $C_1(t)$, $C_2(t)$, $C_3(t)$, $C_4(t)$, $C_5(t)$, $C_6(t)$, $D_1(t)$, $D_2(t)$ and $D_3(t)$, and the vectors $\varrho_1(t)$, $\varrho_2(t)$ are defined as the partial derivatives of the functions f, h, q, k, g_1, and g_2 in (1)-(2), (4), (8)-(10), evaluated along the nominal trajectory (see [15], [20] for the details on the procedure).

In our formulation, we consider $\Delta Q_L = 0$, so we ignore the term $D_2(t)\Delta Q_L$ in (16). We assume the nominal trajectory is well behaved; therefore $C_3(t)$ and $C_6(t)C_3^{-1}(t)C_2(t) - C_5(t)$ are invertible.

The suitability of the use of a 9-state linearized model to capture the effects of uncertainty on system dynamic behavior is shown in [21], where convincing simulations for large deviations in power injections that show that the linearized dynamics is indeed very accurate are presented.

III. Power System Dynamics Stochastic Model

In the linear model described in (11)-(16), we consider three sources of uncertainty arising from (i) load variations, (ii) wind-based generation, and (iii) noise in communication channels. In this section, we develop a stochastic model describing the power system dynamics that captures the impact of the aforementioned uncertainty sources on the system dynamic behavior. In addition, we use the infinitesimal generator model to obtain expressions for moments of system characteristics.

A. Stochastic Differential Equation (SDE) Model

Noise in communication channels introduces uncertainty in the measurements of $\Delta P_{mm'}$, Δf_m and ΔP_{G_i}, which are used as feedback inputs by the AGC system. Let Γ be the vector containing all the $\Delta P_{mm'}$, Δf_m, and ΔP_{G_i}. We denote the measurements of Γ as $\hat{\Gamma}$; then we have that

$$\hat{\Gamma} = \Gamma + \eta, \tag{17}$$

where η is a vector of Gaussian white noise processes. The ACE, as well as the AGC system, are affected by η as one can see in (6) and (7). After including this source of uncertainty in (13), we have that

$$\Delta\dot{z} = A_4(t)\Delta x + A_5(t)\Delta y + A_6(t)\Delta\tilde{y} + A_7(t)\Delta z + A_8(t)\eta. \tag{18}$$

Following [22] and [23], we model load and wind speed variations as stochastic differential equations. Then, we have that

$$d\Delta P_{L_i} = \nu_{1_i}\Delta P_{L_i}dt + \nu_{2_i}dW_t^2, \tag{19}$$

$$d\Delta v_i = a_i\,\Delta v_i\,dt + b_i\,dW_t^3, \tag{20}$$

where W_t^2 and W_t^3 are Wiener processes, and a_i, b_i are parameters constructed based on a priori knowledge of the wind speed pdf. The drift and diffusion parameters in the aforementioned stochastic differential equations are determined with the use of historical data and estimation techniques [24], [25].

In (2) and (10), since $C_3(t)$ and $C_6(t)C_3^{-1}(t)C_2(t) - C_5(t)$ are assumed to be invertible, we can solve for Δy and $\Delta\tilde{y}$. We substitute Δy, $\Delta\tilde{y}$, and Δu in (11) and (19), and obtain the following stochastic differential equation (SDE) model:

$$dX_t = AX_t dt + BdW_t, \tag{21}$$

where $X_t = [\Delta x, \Delta z, \Delta P_L, \Delta P_W, \Delta v]^T$, A, B as defined in the Appendix, and $dW_t = [dW_t^1, dW_t^2, dW_t^3]^T$. We assume that the initial system state is steady; thus, we have $X_0 = 0$.

There are cases in which we wish to represent the deepening penetration of wind generation and the increased level of variability in the output. To this end, we use (3) and assume

that the wind penetration at bus i is now $P'_{W_i} = \xi_i P_{W_i}$. Then, we model the variation in the wind generation as

$$\Delta \dot{P}_{W_i} = \varrho_{1_i} \Delta P_{W_i} + \xi_i \varrho_{2_i} \Delta v_i. \tag{22}$$

We have that $P'_{W_i} = \xi_i P_{W_i} \rightarrow \Delta P'_{W_i} = \xi_i \Delta P_{W_i}$, since the nominal point around which we linearize is now $P'^{\star}_{W_i} = \xi_i P^{\star}_{W_i}$. Thus, we only need to modify a few entries in the B matrix to represent the deepening penetration of renewable-based generation.

B. SDE Infinitesimal Generator

The overall model, as described by the SDE in (21), is used to study the impact of the uncertainty on system dynamic performance. To this end, we use the generator of the process X_t to calculate the statistics of the states of interest. Specifically, given a twice continuously differentiable function ψ, the generator of the process X_t is defined as (see, e.g., [26]):

$$\begin{aligned}(L\psi)(x,t) \quad := \quad & \frac{\partial \psi(x,t)}{\partial t} + \frac{\partial \psi(x,t)}{\partial x} Ax \\ & + \frac{1}{2} \mathrm{Tr}\left(B \frac{\partial^2 \psi(x)}{\partial x^2} B^T \right).\end{aligned} \tag{23}$$

The evolution of the expected value of $\psi(x)$ is governed by Dynkin's formula (see, e.g., [26]):

$$\frac{d\mathbb{E}[\psi(X((t))]}{dt} = \mathbb{E}[(L\psi)(X(t))], \tag{24}$$

where $\mathbb{E}[\cdot]$ denotes the expectation operator. By properly choosing ψ, we may obtain a set of ordinary differential equations (ODEs) the evolution of which describes the desired moments of the dynamic/algebraic states. Therefore, we may study the impact of uncertainty in wind-based generation, load variations and noise in communication channels on the area frequency and the area control error, which in turn are utilized in the computation of the frequency performance criteria.

IV. Impacts on Frequency Performance Criteria

In this section, we introduce the frequency performance metrics developed by NERC, and use the proposed framework in Section III to develop probabilistic expressions of these metrics.

A. Frequency Performance Criteria

NERC has established the CPS1, CPS2, and BAAL performance criteria to quantify whether or not system frequency is maintained within certain limits [4], [5]; next, we provide their definitions

For BA area m, CPS1 is given by

$$\frac{\sum_{i \in \mathscr{T}_1} \langle ACE \rangle_{1_{m_i}} \langle \Delta f \rangle_{1_{m_i}}}{|\mathscr{T}_1|} \leq -b_m \epsilon^2_{1_m}, \tag{25}$$

where $\langle \cdot \rangle_{1_{m_i}}$ denotes the i^{th} average over a 1-minute period for BA area m of each variable respectively, $\mathscr{T}_1$ is the set of time instants for which we have measurements for the 1-minute averages of the frequency deviation from the nominal value, denoted by Δf_m, and the area control error of BA area m, denoted by ACE_m, over a one year period, $|\mathscr{T}_1|$ is the cardinality of the set $\mathscr{T}_1$, and ϵ_{1_m} is a constant unique for each BA area m.

The CPS2 is designed to limit the BA area unscheduled power flows. To this end, CPS2 is given by

$$|\langle ACE \rangle_{10_{m_i}}| \leq \quad L_{10_m}, \tag{26}$$

$$1 - \frac{\text{number of violations of (26)}}{|\mathscr{T}_2|} \geq \quad 0.9, \tag{27}$$

where $\langle \cdot \rangle_{10_{m_i}}$ denotes the i^{th} average over a 10-minute period for BA area m of ACE, $\mathscr{T}_2$ is the set of time instants for which we have measurements for the 10-minute averages of ACE_m over a one month period, $|\mathscr{T}_2|$ is the cardinality of the set $\mathscr{T}_2$, and L_{10_m} a constant specific for each BA area m.

The BAAL criterion, which will replace the CPS2 criterion [5], may be formulated as follows

$$BAAL_{\text{low}}(f_m) = -b_m \frac{(f_{\text{low}} - f_{\text{nom}})^2}{f_m - f_{\text{nom}}}, \tag{28}$$

$$BAAL_{\text{high}}(f_m) = -b_m \frac{(f_{\text{high}} - f_{\text{nom}})^2}{f_m - f_{\text{nom}}}. \tag{29}$$

For each violation, the BAAL standard allows a BA area to have its ACE outside the BAAL limits for a certain time, which is 30 min.

B. Probabilistic Expression of Frequency Metrics

We use the framework developed in Section III to derive probabilistic expressions for the three frequency performance criteria given in (25)-(29). To this end, we express the ACE of BA area m, ACE_m, and the deviation of the area frequency from the nominal value, Δf_m, as functions of the system states X_t. We linearize (5) and (6) along the nominal trajectory, and obtain

$$\Delta f_m = \Phi_{1_m} X_t, \tag{30}$$

$$ACE_m = \Phi_{2_m} X_t. \tag{31}$$

We wish to obtain the pdfs of ACE_m and Δf_m. Since the overall model given in (21) is driven by a Wiener process, then the system state, X_t, follows a Gaussian distribution [27]. Thus, only the first and second moments are needed to obtain the pdf of X_t. Both ACE_m and Δf_m are linear combinations of X_t, so they also follow a Gaussian distribution. We use (24) to obtain the first and second moments of ACE_m and Δf_m by appropriately selecting the function $\psi(\cdot)$. For example, with $\psi(X_t) = \Phi_{2_m} X_t$ we may obtain the first moment of $ACE_m(t)$, which is zero, since $\psi(X_t)$ is time invariant and linear with respect to X_t. For $\psi(X_t) = \Phi_{2_m} X_t X_t^T \Phi_{2_m}^T$, we may obtain the second moment of $ACE_m(t)$, which we denote by σ^2_{ACE}. Then, ACE_m follows a Gaussian distribution with zero mean and variance σ^2_{ACE}.

We note that the variables included in (25)-(27) are time averages of either ACE_m or Δf_m, so we need to determine the pdfs of these variables, given that we have the pdfs of ACE_m and Δf_m. We show the derivation for X_t, since both ACE_m and Δf_m are linear combinations of X_t. The vector X_t follows a Gaussian distribution with zero mean and covariance matrix Σ_X, which can be obtained using

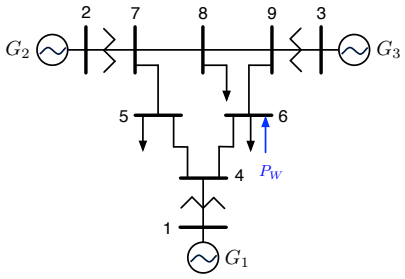

Fig. 1: One-line diagram of the 3-machine 9-bus power system.

Dynkin's formula, as given in (24). Consider a time interval $[t_s, t_e]$, we choose a window of length L and define the subinterval $\mathscr{T}^i = [t_s+(i-1)L, t_s+iL]$, $i = 1, \ldots, N$, where $N = \frac{t_e-t_s}{L}$. For each subinterval, we define the measurement subset $\mathscr{M}^i = \{t_j, j = 1, \ldots, J\}$. For the 1-minute average, with $L = 1$ min, we have the average $\langle X\rangle_{1_i}$, and for the 10-minute average, with $L = 10$ min, we have $\langle X\rangle_{10_i}$. We now have that

$$\langle X\rangle_{L_i} = \frac{1}{J}\sum_{t_j\in\mathscr{M}^i} X(t_j), i = 1, \ldots, N. \tag{32}$$

In order to determine the pdf of the L-minute averages of X_t, we use the central limit theorem for dependent variables [28]. The cardinality J of each $\mathscr{M}^i$ is sufficiently large so as to allow the application of the central limit theorem. Thus, we have that $\langle X\rangle_{L_i}$ follows a Gaussian distribution with zero mean and covariance matrix Σ_L, the elements of which consist of combinations of the elements of the matrices $\mathbb{E}[X(t_i)X^T(t_i)]$ and $\mathbb{E}[X(t_i)X^T(t_j)]$, for $i, j = 1, \ldots, J$. We know that the value of $\mathbb{E}[X(t_i)X^T(t_i)]$ is Σ_X; then, in order to determine the values of $\mathbb{E}[X(t_i)X^T(t_j)]$, for $i, j = 1, \ldots, J$ with $i \neq j$, we use the fact that X_t is a wide-sense stationary process (see, e.g., [29]). Therefore, we have that $\mathbb{E}[X(t_i)X^T(t_j)] = \mathbb{E}[X(t_i - t_j)X^T(t_i - t_j)]$, and we use the fact that $\mathbb{E}[X(t_i - t_j)X^T(t_i - t_j)] = e^{A(t_j-t_i)}\mathbb{E}[X(t_i)X^T(t_i)] = e^{A(t_j-t_i)}\Sigma_X$, for $t_i < t_j$ [27]. We use this procedure and obtain the pdfs of $\langle ACE\rangle_{1_{m_i}}$, $\langle \Delta f\rangle_{1_{m_i}}$, and $\langle ACE\rangle_{10_{m_i}}$. For example, $\langle ACE\rangle_{1_{m_i}}$ follows a Gaussian distribution with zero mean and variance $\sigma^2_{\langle ACE\rangle_1}$, which is equal to $\Phi_{2_m}\Sigma_1\Phi^T_{2_m}$ (Σ_1 is the covariance matrix of $\langle X\rangle_{1_i}$).

Furthermore, we assume that the elements of the discrete-time stochastic process $\{\langle X\rangle_{L_i}, i = 1, \ldots, N\}$ are independent and identically distributed random variables, thus ergodic. So its statistical properties (such as mean and variance) may be deduced from a single, sufficiently long realization. Thus, CPS1 is equivalent to

$$\Phi_{2_m}\mathbb{E}[\langle X\rangle_1\langle X\rangle_1^T]\Phi^T_{1_m} < -b_m\epsilon^2_{1_m}, \tag{33}$$

where $\mathbb{E}[\langle X\rangle_1\langle X\rangle_1^T] = \Sigma_1$. As for CPS2 we define the variable

$$\Upsilon_i = \begin{cases} 1, & |\langle ACE\rangle_{10_{m_i}}| < L_{10_m} \\ 0, & \text{otherwise} \end{cases}, \text{ for } i = 1, \ldots, N, \tag{34}$$

So CPS2 may be written as: $\mathbb{E}[\Upsilon_i] = \Pr\{|\langle ACE\rangle_{10_{m_i}}| < L_{10_m}\} = \Pr\{\langle ACE\rangle_{10_{m_i}} < L_{10_m}\} - \Pr\{\langle ACE\rangle_{10_{m_i}} < -L_{10_m}\} \geq 0.9$, which may be easily calculated since $\langle ACE\rangle_{10_{m_i}}$ follows a Gaussian distribution with known mean and variance.

From (28)-(29), we may rewrite the BAAL criterion as $-b_m(f_{\text{low}} - f_{\text{nom}})^2 \leq \frac{\sum_{t\in\mathscr{T}_3} ACE_m(t)\Delta f_m(t)}{|\mathscr{T}_3|} \leq -b_m(f_{\text{high}} - f_{\text{nom}})^2$, where $\mathscr{T}_3$ is the set of time instants for which we have measurements for $ACE_m(t)$ and $\Delta f_m(t)$ for a 30-minute period; however, we may express $ACE_m(t)$ and $\Delta f_m(t)$ as a function of X_t. We assume that the statistical properties (such as its mean and variance) of the process may be deduced from a single, sufficiently long realization. So equivalently, we have that $\frac{\sum_{t\in\mathscr{T}_3} ACE_m(t)\Delta f_m(t)}{|\mathscr{T}_3|} = \mathbb{E}[ACE_m(t)\Delta f_m(t)] = \Phi_{2_m}\mathbb{E}[X_tX_t^T]\Phi^T_{1_m}$. Then, the BAAL may be expressed as

$$\begin{aligned} b_m^2(f_{\text{low}} - f_{\text{nom}})^2 &\leq \Phi_{2_m}\mathbb{E}[X_tX_t^T]\Phi^T_{1_m} \\ &\leq b_m^2(f_{\text{high}} - f_{\text{nom}})^2. \end{aligned} \tag{35}$$

V. Numerical Examples

We present several numerical examples to demonstrate the capabilities of the proposed framework. We use a small system, the WECC three-machine nine-bus system, to provide insights into the results presented. We demonstrate that the pdfs calculated by using Dynkin's formula as well as the pdfs for the 1-minute and for 10-minute average of the system variables match the results we obtain via Monte Carlo simulations of the DAE system given in (1)-(2), (4), (8)-(10). Additionally, the probabilistic expression of the frequency performance criteria provides a good approximation of the actual frequency performance metrics. Furthermore, we include a larger system, with 48 machines and 140 buses, to illustrate the scalability of the proposed method.

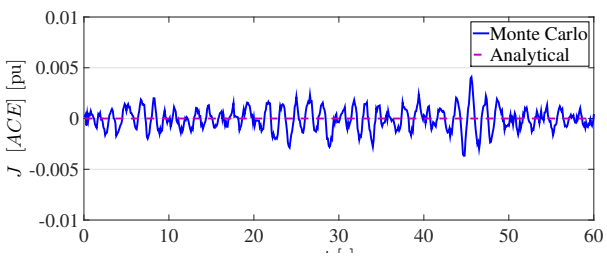

(a) Mean value of ACE.

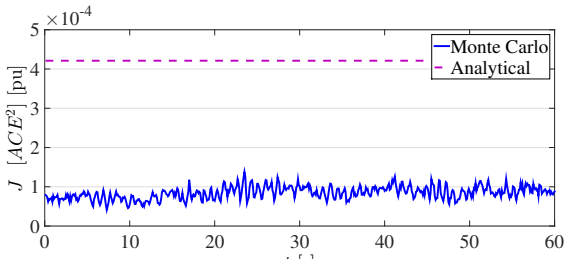

(b) Second moment of ACE.

Fig. 2: First and second moment of ACE.

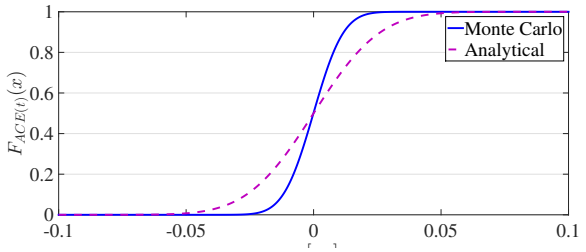

Fig. 3: Cumulative distribution function of $ACE(t)$, $P(ACE(t) \leq x) \equiv F_{ACE(t)}(x)$.

A. Three-Machine Nine-Bus Power System

Consider the WECC three-machine nine-bus power system model, which is depicted in Fig. 1; this model contains three synchronous generating units in buses 1, 2 and 3, and load in buses 5, 6 and 8. Additionally, we introduce wind-based generation at bus 6. Unless otherwise noted, all quantities in this section are expressed in per unit (pu) with respect to 100 MVA as base power. The machine, network and load parameter values may be found in [15, pp. 170-172]. We consider one BA area for the system and choose the frequency bias factor to be $b = -1.152$ pu/Hz. The AGC participation factors are $\kappa_1 = 0.28$, $\kappa_2 = 0.47$ and $\kappa_3 = 0.25$.

We solve the power flow equations and the machine algebraic equations such that the wind generation in bus 6 is $P_{W_6} = 0.298$, the load in bus 5 is $P_{L_5} + jQ_{L_5} = 1.25 + j0.50$, in bus 6 is $P_{L_6} + jQ_{L_6} = 0.90 + j0.30$ and in bus 8 is $P_{L_8} + jQ_{L_8} = 1.50 + j0.35$. We consider the generator in bus 1 as the slack bus. We linearize the DAE system around the nominal point determined by solving the algebraic equations.

Noise in communication channels is modeled as a Gaussian distribution with zero mean and variance 0.01. The load variation is given by

$$\begin{aligned} d\Delta P_{L_i} &= -2 \cdot 10^{-6} \Delta P_{L_i} dt \\ &\quad + 5 \cdot 10^{-3} dW_t^2, \text{ for } i = 5, 6, 8. \end{aligned} \tag{36}$$

The variation of the wind generation output in bus 6 is ΔP_{W_6} and its evolution is described by

$$\Delta \dot{P}_{W_6} = -0.1585 \Delta P_{W_6} + 0.0118 \Delta v_6, \tag{37}$$

where the variation in the wind speed Δv_6 is described by the stochastic process $d\Delta v_6 = -2.65 \cdot 10^{-4} \Delta v_6 dt + 1.62 \cdot 10^{-2} dW_t^3$. We use the Euler-Maruyama method to obtain paths of the stochastic differential equations (see, e.g., [30]).

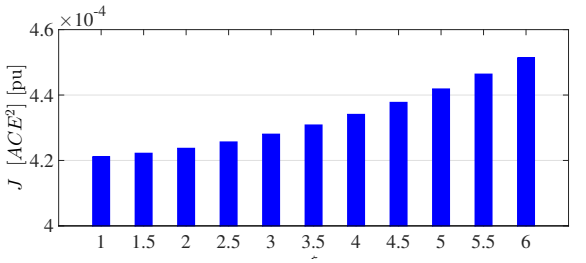

Fig. 4: Deepening wind penetration.

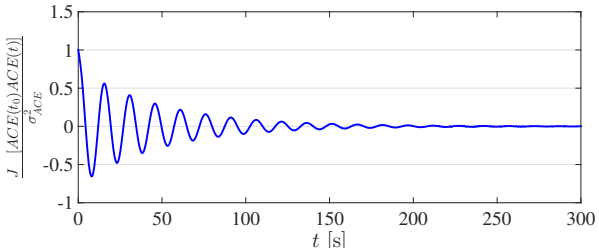

Fig. 5: Correlation of ACE.

1) SDE infinitesimal generator: We use Dynkin's formula as given in (24), with $\psi(X_t) = \Phi_2 X_t$ and $\psi(X_t) = \Phi_2 X_t X_t^T \Phi_2^T$, to calculate the mean value and the second moment of ACE, respectively; the results are depicted in Fig. 2. The results obtained with the proposed framework are superimposed to those calculated by averaging the results of 1000 Monte Carlo simulations at each time instant. The results provided by the analytical method, i.e., Dynkin's formula, provide a good approximation compared to those obtained by averaging the results of repeated simulations. We notice that in this case, the AGC system meets its objective, since the mean value of ACE, $\mathbb{E}[ACE]$, converges to zero and its second uncentered moment, $\mathbb{E}[ACE^2]$, converges to $4.211 \cdot 10^{-4}$. Since ACE follows a Gaussian distribution, and we know its first and second moments, we may determine its pdf.

We use the data from repetitive Monte Carlo simulations, to derive an empirical cumulative distribution function (cdf) of $ACE(t)$ and compare it with the cdf from the analytical approach; the results are depicted in Fig. 3. We notice that the analytical method provides a larger standard deviation for ACE than that obtained via Monte Carlo simulations. In the proposed framework, the linearized model, given in (11)-(16), is used, whereas, in the Monte Carlo simulations the DAE model, given in (1)-(2), (4), (8)-(10), is used; that is the reason for the discrepancy in the results, as shown in Fig. 3. As a result, the effects of uncertainty sources on the system are magnified with the analytical approach, which may lead to more conservative actions from the system operators. However, the analytical method provides a good approximation, and results in faster computations.

We now investigate the effects on ACE of deepening renewable-based generation, as described in (22). More specifically, we increase the wind penetration from the initial value $P_{W_6} = 0.298$ to $P'_{W_6} = \xi P_{W_6}$, where the parameter ξ belongs in $[1, 6]$ and is modified in increments of 0.5. We observe

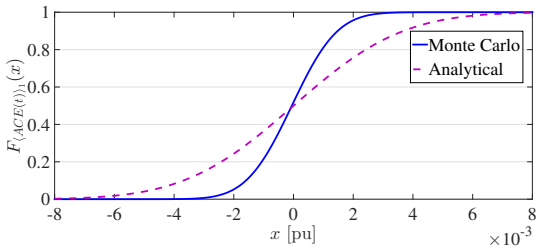

Fig. 6: Cumulative distribution function of $\langle ACE(t)\rangle_1$, $P(\langle ACE(t)\rangle_1 \leq x) \equiv F_{\langle ACE(t)\rangle_1}(x)$.

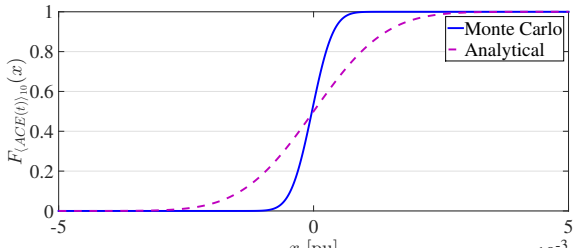

Fig. 7: Cumulative distribution function of $\langle ACE(t)\rangle_{10}$, $P(\langle ACE(t)\rangle_{10} \leq x) \equiv F_{\langle ACE(t)\rangle_{10}}(x)$.

that the second moment of ACE is higher as we increase the wind penetration levels, as shown in Fig. 4; renewable-based generation introduces variability and uncertainty to the system, which is reflected in ACE.

2) Frequency performance metrics: We have shown that the proposed framework provides a good approximation of the system behavior, as validated via extensive Monte Carlo simulations of the non-linear system dynamics. In order to calculate the values for the frequency performance criteria, we need to determine the pdfs of the 1-minute and 10-minute averages of the system variables.

In this case study, we consider only one BA area, thus the frequency deviation and ACE are proportional to each other, i.e., $ACE = -b\Delta f$; therefore, the vectors Φ_1 and Φ_2, are related as follows: $\Phi_1 = \frac{1}{-b}\Phi_2$. The frequency criteria may be expressed as a function of the characteristics of ACE, 1-minute average of ACE, denoted by $\langle ACE\rangle_1$, and 10-minute average of ACE, denoted by $\langle ACE\rangle_{10}$, if we substitute Φ_1 in the equations of Section IV with $\Phi_1 = \frac{1}{-b}\Phi_2$. We first need to calculate the correlation of $ACE(t_i)$ and $ACE(t_j)$ for some i, j with $t_j > t_i$, i.e., $\mathbb{E}[ACE(t_i)ACE(t_j)] = \Phi_2\mathbb{E}[X_{t_i}X_{t_i}^T]e^{A(t_j-t_i)}\Phi_2^T$. We depict the correlation for $ACE(t_0 = 0)$ with $ACE(t)$, $t > 0$ in Fig. 5. We notice that the correlation of $ACE(t_1)$ and $ACE(t_k)$ drops significantly for $|t_1 - t_k| > 300s$. The negative correlation between the random variables is due to the eigenvectors of matrix A, which is negative definite; thus, the correlation values converge to zero. We use the central limit theorem for dependent variables and find that $\langle ACE(t)\rangle_1$, the 1-minute average of ACE, follows a Gaussian distribution with zero mean and variance $8.27 \cdot 10^{-6}$, and that $\langle ACE(t)\rangle_{10}$, the 10-minute average of ACE, follows a Gaussian distribution with zero mean and variance $1.15 \cdot 10^{-6}$.

We use the data from Monte Carlo simulations, calculate the 1-minute and 10-minute averages, and derive empirical cdfs of

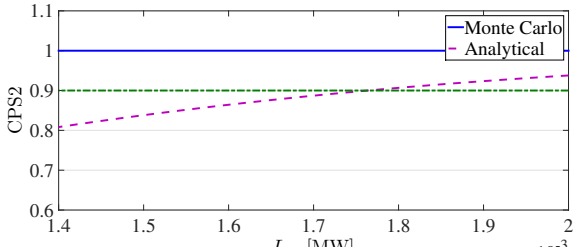

Fig. 8: Sensitivity of CPS2 with respect to changes in L_{10}.

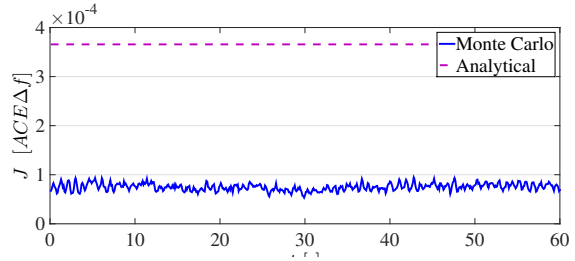

Fig. 9: BAAL criterion: $\frac{\sum_{t\in\mathcal{T}_3} ACE_m(t)\Delta f_m(t)}{|\mathcal{T}_3|}$.

$\langle ACE(t)\rangle_1$ and $\langle ACE(t)\rangle_{10}$, which we compare to the cdfs of the Gaussian distributions from the analytical approach, as shown in Figs. 6 and 7. As in the case for ACE, the standard deviations for the 1-minute and 10-minute averages are higher with the analytical approach. This is due to the fact that the error introduced in $ACE(t)$ is propagated to $\langle ACE(t)\rangle_1$ and $\langle ACE(t)\rangle_{10}$.

Based on the analysis in Section IV, we calculate the values of the frequency performance criteria. CPS1 criterion is equal to $\frac{1}{-b}\mathbb{E}[\langle ACE\rangle_1^2(t)] = \frac{1}{1.152}8.27 \cdot 10^{-6} = 7.179 \cdot 10^{-6}$. We use Monte Carlo simulations and calculate CPS1 based on (25); thus, we have that CPS1 is $6.799 \cdot 10^{-6}$. As for CPS2, we modify the value of L_{10}, i.e., how restrictive CPS2 is, and show the sensitivity of the proposed method with respect to L_{10}, as depicted in Fig. 8. We notice that the proposed framework shows that CPS2 is violated, i.e., is less than 0.9, in cases where Monte Carlo simulations indicated otherwise. However, the values of L_{10} corresponding to such cases were very small, i.e., CPS2 is very restrictive, and for larger values of L_{10}, which are more realistic values for this particular system, the results from the analytical approach and the Monte Carlo simulations are close and agree that no violations are present. For the BAAL criterion, we need to calculate the values of $\mathbb{E}[ACE\Delta f]$. We know that $ACE = -b\Delta f$, thus $\mathbb{E}[ACE\Delta f] = \frac{\mathbb{E}[ACE^2]}{-b}$. We compare the value obtained from the analytical method with the results from the Monte Carlo simulations for $\frac{\sum_{t\in\mathcal{T}_3} ACE_m(t)\Delta f_m(t)}{|\mathcal{T}_3|}$, where $\mathcal{T}_3$ corresponds to a 30-minute period. We depict the results in Fig. 9.

The probabilistic expressions of the frequency performance criteria provide a good approximation to those calculated via simulations of the DAE model. The analytical method magnifies the effects of the sources of uncertainty considered; however its advantage is computational efficiency, which makes the introduced error acceptable. In order to quantify the effects of uncertainty sources on the system performance based

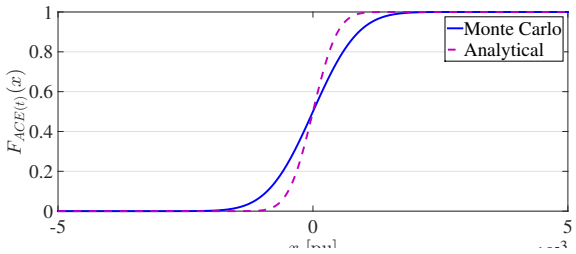

Fig. 10: Cumulative distribution function of $ACE(t)$, $P(ACE(t) \leq x) \equiv F_{ACE(t)}(x)$.

on historical data we need to run simulations for an entire year in the case of CPS1. In contrast, by using the proposed framework and the probabilistic expression of the frequency performance criteria, we only need to solve a system of ODEs.

B. 140-Bus System

Next, we demonstrate the scalability of the proposed methodology for large power systems. In particular, we utilize the IEEE 48-machine test system, which consists of 140 buses and 233 lines [31]. To implement our analysis method, we use the MATLAB-based Power Systems Toolbox (PST) [32], and add the AGC system model described in (8)-(9) to it. We use the proposed framework to calculate the values for the frequency performance criteria and compare them with the results obtained via Monte Carlo simulations.

We consider three sources of uncertainty, namely, load variation, renewable-based generation, and noise in communication channels. Load variation and renewable-based generation are modeled as Wiener processes without scaling and drift, and noise in communication channels as white noise. Wind-based generation is placed at load bus 1. We consider the entire system as one BA area, and we set the frequency bias factor for the AGC system at -1 pu. The AGC participation factors are set proportional to the inertia constants of the generators.

We obtain the linear model with the help of the PST, and determine the matrices A and B in (21). We use Dynkin's formula to obtain the first and second moment of ACE and approximate its cdf. In Fig. 10, we compare the cdf obtained with Dynkin's formula, with the empirical cdf of ACE determined by numerous Monte Carlo simulations of the DAE model. The value of CPS1 is $0.751 \cdot 10^{-8}$ calculated with the proposed framework and $1.711 \cdot 10^{-8}$ with simulations of the non-linear system, respectively. We notice that the proposed framework provides a good approximation as also established in the smaller test system.

VI. Concluding Remarks

In this paper, we developed a framework for studying the impact on AGC system performance of uncertainty that arises from load variations, renewable-based power generation and noise in communication channels. Through the numerical examples, we showed that Dynkin's formula provides a good approximation of the system actual state, as validated with repetitive Monte Carlo simulations.

In order to find the limiting values of uncertainty that the system may withstand and maintain the desired reliability levels, we used the proposed framework to obtain probabilistic expressions of the frequency performance criteria. These expressions may be utilized to investigate the needs for new designs in AGC systems due to the changes in the electric grid.

There are natural extensions of the work presented here. For instance, there are other communication problems, besides noise, in the communication channels, such as communication delay, bit error and communication interruption. In our future studies, we plan on studying the impacts of the aforementioned communication problems on AGC systems. In addition, we will investigate the possibility of using the non-linear system to propagate uncertainty from the input sources to system states, in order to avoid the errors introduced due to the use of the linear system. We will report on these developments in future papers.

Appendix

The vectors for the uncertainty models in (3), (19), and (20), the matrices for the SDE in (21) are defined as

$\varrho_1 = [\varrho_{1_1}, \ldots, \varrho_{1_n}]^T$, $\varrho_2 = [\varrho_{2_1}, \ldots, \varrho_{2_n}]^T$,
$a = [a_1, \ldots, a_n]^T$, $b = [b_1, \ldots, b_n]^T$,
$\nu_1 = [\nu_{1_1}, \ldots, \nu_{1_n}]^T$, $\nu_2 = [\nu_{2_1}, \ldots, \nu_{2_n}]^T$,

$$A = \begin{bmatrix} A_{11} & A_{12} & A_{13} & A_{14} & A_{15} \\ A_{21} & A_{22} & A_{23} & A_{24} & A_{25} \\ A_{31} & A_{32} & A_{33} & A_{34} & A_{35} \\ A_{41} & A_{42} & A_{43} & A_{44} & A_{45} \\ A_{51} & A_{52} & A_{53} & A_{54} & A_{55} \end{bmatrix},$$

$$B = \begin{bmatrix} B_{11} & B_{12} & B_{13} \\ B_{21} & B_{22} & B_{23} \\ B_{31} & B_{32} & B_{33} \\ B_{41} & B_{42} & B_{43} \\ B_{51} & B_{52} & B_{53} \end{bmatrix},$$

with

$$\begin{aligned}
A_{11} &= A_1 + A_2(C_6C_3^{-1}C_2 - C_5)^{-1}(C_4 - C_6C_3^{-1}C_1) \\
&\quad - A_3\{C_3^{-1}C_1 \\
&\quad + C_3^{-1}C_2(C_6C_3^{-1}C_2 - C_5)^{-1}(C_4 - C_6C_3^{-1}C_1)\}, \\
A_{12} &= B_1B_2, \\
A_{13} &= A_2(C_6C_3^{-1}C_2 - C_5)^{-1}D_1 \\
&\quad - A_3C_3^{-1}C_2(C_6C_3^{-1}C_2 - C_5)^{-1}D_1, \\
A_{14} &= A_2(C_6C_3^{-1}C_2 - C_5)^{-1}D_3 \\
&\quad - A_3C_3^{-1}C_2(C_6C_3^{-1}C_2 - C_5)^{-1}D_3, \\
A_{15} &= 0_{9I-1\times n}, \\
A_{21} &= A_4 - A_6(C_3^{-1}C_2(C_6C_3^{-1}C_2 - C_5)^{-1}(C_4 - C_6C_3^{-1}C_1) \\
&\quad + C_3^{-1}C_1) + A_5(C_6C_3^{-1}C_2 - C_5)^{-1}(C_4 - C_6C_3^{-1}C_1), \\
A_{22} &= A_7, \\
A_{23} &= A_5(C_6C_3^{-1}C_2 - C_5)^{-1}D_1 \\
&\quad - A_6C_3^{-1}C_2(C_6C_3^{-1}C_2 - C_5)^{-1}D_1, \\
A_{24} &= A_5(C_6C_3^{-1}C_2 - C_5)^{-1}D_3 \\
&\quad - A_6C_3^{-1}C_2(C_6C_3^{-1}C_2 - C_5)^{-1}D_3, \\
A_{25} &= 0_{M\times n}, \\
A_{31} &= 0_{n\times 9I-1},\ A_{32} = 0_{n\times M},\ A_{33} = diag(\nu_1), \\
A_{34} &= 0_{n\times n},\ A_{35} = 0_{n\times n},\ A_{41} = 0_{n\times 9I-1}, \\
A_{42} &= 0_{n\times M},\ A_{43} = 0_{n\times n},\ A_{44} = diag(\varrho_1), \\
A_{45} &= diag(\varrho_2),\ A_{51} = 0_{n\times 9I-1},\ A_{52} = 0_{n\times M}, \\
A_{53} &= 0_{n\times n},\ A_{54} = 0_{n\times n},\ A_{55} = diag(a), \\
B_{11} &= B_{12} = B_{13} = 0_{9I-1\times 1},\ B_{21} = A_8, \\
B_{22} &= B_{23} = 0_{M\times 1},\ B_{31} = B_{33} = 0_{n\times 1},\ B_{23} = \nu_2, \\
B_{41} &= B_{42} = B_{43} = 0_{n\times 1},\ B_{51} = B_{52} = 0_{n\times 1}, \\
B_{53} &= diag(b).
\end{aligned}$$

REFERENCES

[1] "Electricity grid modernization: Progress being made on cyber security guidelines, but key challenges remain to be addressed," Tech. Rep. GAO-11-117, Jan. 2011.

[2] (2014, Accessed Oct.) Renewable portfolio standards. [Online]. Available: www.dsireusa.org

[3] Y. Huang, A. A. Cardenas, and S. Sastry, "Understanding the physical and economic consequences of attacks on control systems," *Elsevier, International Journal of Critical Infrastructure Protection*, vol. 2, no. 3, pp. 72–83, Oct. 2009.

[4] (2014, Accessed Oct.) Real power balancing control performance, BAL-001-1. [Online]. Available: http://www.nerc.com

[5] (2014, Accessed Oct.) Real power balancing control performance, BAL-001-2. [Online]. Available: http://www.nerc.com

[6] D. H. Curtice and T. W. Reddoch, "An assessment of load frequency control impacts caused by small wind turbines," *IEEE Transactions on Power Apparatus and Systems*, vol. PAS-102, no. 1, pp. 162–170, Jan. 1983.

[7] Y. Xiaofeng and K. Tomsovic, "Application of linear matrix inequalities for load frequency control with communication delays," *IEEE Transactions on Power Systems*, vol. 19, no. 3, pp. 1508–1515, Aug. 2004.

[8] P. Esfahani, M. Vrakopoulou, K. Margellos, J. Lygeros, and G. Andersson, "A robust policy for automatic generation control cyber attack in two area power network," in *49th IEEE Conference on Decision and Control (CDC)*, Dec. 2010, pp. 5973–5978.

[9] T. Yu, B. Zhou, K. W. Chan, L. Chen, and B. Yang, "Stochastic optimal relaxed automatic generation control in non-Markov environment based on multi-step Q(λ) learning," *IEEE Transactions on Power Systems*, vol. 26, no. 3, pp. 1272–1282, Aug. 2011.

[10] Q. Liu and M. D. Ilic, "Enhanced automatic generation control (E-AGC) for future electric energy systems," in *IEEE Power and Energy Society General Meeting*, Jul. 2012, pp. 1–8.

[11] K. Wang and M. L. Crow, "The Fokker-Planck equation for power system stability probability density function evolution," *IEEE Transactions on Power Systems*, vol. 28, no. 3, pp. 2994–3001, Aug. 2013.

[12] F. Milano and R. Zarate-Minano, "A systematic method to model power systems as stochastic differential algebraic equations," *IEEE Transactions on Power Systems*, vol. 28, no. 4, pp. 4537–4544, Nov. 2013.

[13] S. V. Dhople, Y. C. Chen, L. DeVille, and A. D. Domínguez-García, "Analysis of power system dynamics subject to stochastic power injections," *IEEE Transactions on Circuits and Systems I: Regular Papers*, vol. 60, no. 12, pp. 3341–3353, Dec. 2013.

[14] L.-R. Chang-Chien, C.-C. Sun, and Y.-J. Yeh, "Modeling of wind farm participation in AGC," *IEEE Transactions on Power Systems*, vol. 29, no. 3, pp. 1204–1211, May 2014.

[15] P. W. Sauer and M. A. Pai, *Power System Dynamics and Stability*. Upper Saddle River, NJ: Prentice Hall, 1998.

[16] H. A. Pulgar-Painemal and P. W. Sauer, "Towards a wind farm reduced-order model," *Electric Power Systems Research*, vol. 81, no. 8, pp. 1688–1695, 2011.

[17] A. Wood and B. Wollenberg, *Power Generation, Operation, and Control*. New York, NY: Wiley, 1996.

[18] L. Wang and D. Chen, "Extended term dynamic simulation for AGC with smart grids," in *IEEE Power and Energy Society General Meeting*, Jul. 2011, pp. 1–7.

[19] D. Apostolopoulou, P. W. Sauer, and A. D. Domínguez-García, "Automatic generation control and its implementation in real time," in *47th Hawaii International Conference on System Sciences (HICSS)*, Jan. 2014, pp. 2444–2452.

[20] A. D. Domínguez-García, "Models for impact assessment of wind-based power generation on frequency control," in *Control and Optimization Methods for Electric Smart Grids, Power Electronics and Power Systems*, M. Ilić and A. Chakrabortty, Eds. New York, Springer, 2012.

[21] Y. C. Chen and A. D. Domínguez-García, "A method to study the effect of renewable resource variability on power system dynamics," *IEEE Transactions on Power Systems*, vol. 27, no. 4, pp. 1978–1989, Nov. 2012.

[22] M. Perninge, M. Amelin, and V. Knazkins, "Load modeling using the Ornstein-Uhlenbeck process," in *IEEE 2nd International Power and Energy Conference*, Dec. 2008, pp. 819–821.

[23] K. Wang and M. Crow, "Fokker-Planck equation application to analysis of a simplified wind turbine model," in *North American Power Symposium (NAPS)*, Sep. 2012, pp. 1–5.

[24] A. R. Pedersen, "A new approach to maximum likelihood estimation for stochastic differential equations based on discrete observations," *Scandinavian Journal of Statistics*, vol. 22, no. 1, pp. 55–71, Mar. 1995.

[25] A. W. Lo, "Maximum likelihood estimation of generalized Itô processes with discretely sampled data," *Econometric Theory*, vol. 4, no. 2, pp. 231–247, Aug. 1988. [Online]. Available: http://www.jstor.org/stable/3532294

[26] B. Øksendal, *Stochastic Differential Equations: An Introduction with Applications*. New York, Springer, 2010.

[27] C. K. I. Williams, "A tutorial introduction to stochastic differential equations: Continuous time Gaussian Markov processes," in *NIPS Workshop on Dynamical Systems, Stochastic Processes and Bayesian Inference*, Dec. 2006.

[28] W. Hoeffding and H. Robbins, "The central limit theorem for dependent random variables," *Duke Mathematical Journal*, vol. 15, no. 3, pp. 773–780, Sep. 1948.

[29] "Stochastic processes and linear dynamic system models," in *Stochastic models, estimation, and control*, ser. Mathematics in Science and Engineering, P. S. Maybeck, Ed. Elsevier, 1979, vol. 141, Part 1, pp. 133–202.

[30] P. Kloeden and E. Platen, *Numerical Solution of Stochastic Differential Equations*, ser. Applications of Mathematics. New York, Springer-Verlag, 1992.

[31] (2014, Accessed Oct.) Power system test case archive, University of Washington. [Online]. Available: http://www.ee.washington.edu/research/ pstca/

[32] (2014, Accessed Oct.) Power system toolbox. [Online]. Available: http://www.eps.ee.kth.se/personal/vanfretti/pst

Dimitra Apostolopoulou was awarded a Ph.D. and a M.S. in Electrical and Computer Engineering from University of Illinois at Urbana-Champaign in 2014 and 2011, respectively. She received her undergraduate degree in Electrical and Computer Engineering from National Technical University of Athens, Greece in 2009. She currently works in the Smart Grid and Technology Department at Commonwealth Edison Company. Priorly, she was a Postdoctoral Research Associate at University of Illinois at Urbana-Champaign. Her research interests include power system operations and control, market design and economics.

Alejandro D. Domínguez-García received the degree of "Ingeniero Industrial" from the University of Oviedo (Spain) in 2001 and the Ph.D. degree in electrical engineering and computer science from the Massachusetts Institute of Technology, Cambridge, MA, in 2007.

He is an Associate Professor in the Electrical and Computer Engineering Department at the University of Illinois at Urbana-Champaign, where he is affiliated with the Power and Energy Systems area; he also has been a Grainger Associate since August 2011. He is also an Associate Research Professor in the Coordinated Science Laboratory and in the Information Trust Institute, both at the University of Illinois at Urbana-Champaign.

His research interests are in the areas of system reliability theory and control, and their applications to electric power systems, power electronics, and embedded electronic systems for safety-critical/fault-tolerant aircraft, aerospace, and automotive applications.

Dr. Domínguez-García received the National Science Foundation CAREER Award in 2010, and the Young Engineer Award from the IEEE Power and Energy Society in 2012. In 2014, he was invited by the National Academy of Engineering to attend the U.S. Frontiers of Engineering Symposium, and selected by the University of Illinois at Urbana-Champaign Provost to receive a Distinguished Promotion Award. In 2015, he received the U of I College of Engineering Dean's Award for Excellence in Research.

He is an editor of the IEEE TRANSACTIONS ON POWER SYSTEMS and the IEEE POWER ENGINEERING LETTERS.

Peter W. Sauer (S 73, M 77, SM 82, F 93, LF 12) obtained his Bachelor of Science degree in Electrical Engineering from the University of Missouri at Rolla in 1969, the Master of Science and Ph.D. degrees in Electrical Engineering from Purdue University in 1974 and 1977 respectively. From 1969 to 1973, he was the electrical engineer on a design assistance team for the Tactical Air Command at Langley Air Force Base, Virginia. From August 1991 to August 1992 he served as the Program Director for Power Systems in the Electrical and Communication Systems Division of the National Science Foundation in Washington D.C. He is a cofounder of the Power Systems Engineering Research Center (PSERC) and the PowerWorld Corporation. He is a registered Professional Engineer in Virginia and Illinois, a Fellow of the IEEE, and a member of the U.S. National Academy of Engineering. He is currently the Grainger Chair Professor of Electrical Engineering at Illinois.